DOI: 10.31276/VJSTE.65(3).08-13

Development of a PCB-based passive capacitive sensor for fluidic flow detection

Nhu Cuong Nguyen[1], Bao Anh Hoang[1], Trung Kien Do[2], Thanh Tung Bui[1], Duc Trinh Chu[1], Quang Loc Do[2*]

[1]*Faculty of Electronics and Telecommunications, VNU University of Engineering and Technology, 144 Xuan Thuy Street, Dich Vong Hau Ward, Cau Giay District, Hanoi, Vietnam*
[2]*Faculty of Physics, VNU University of Science, 334 Nguyen Trai Street, Thanh Xuan Trung Ward, Thanh Xuan District, Hanoi, Vietnam*

Received 24 August 2022; revised 26 September 2022; accepted 3 October 2022

Abstract:

A passive wireless sensor system integrated with capacitive fluidic flow detection is proposed and developed based on the printed circuit board (PCB) technique. The capacitive sensing structure consists of PCB-based electrodes enclosing an insulating pipe that contains the fluidic flow of interest. The conductivity of the fluidic flow and the appearance of foreign objects within the flow can be determined by analysing the resonant frequency of the detection path in the proposed system. Experimental results demonstrate that the resonant frequency increases according to the increase in electrical conductivity of the fluidic flow. In addition, the sensing performance is also confirmed by the detection of sizes and electrical conductivities of NaCl droplets passing through the detection zone. Furthermore, this work indirectly verifies the effectiveness and feasibility of the integration of passive wireless sensing technique into the fluidic flow detector by using the PCB fabrication technique and demonstrates great potential for use in various applications in biomedical and chemical fields, especially in biomedical applications.

Keywords: **fluidic flow detection, passive capacitive detection, printed circuit board.**

Classification numbers: **2.1, 2.3**

1. Introduction

Fluidic flow detection refers to the measurement and detection of the properties of fluidic flow including conductivity, permittivity, and the appearance of foreign objects inside the fluidic flow. This technique has become an integral part of several systems in pharmaceutical [1], chemical analysis [2, 3], and biomedical systems [4]. Due to its vital roles in these fields, several methods have been proposed to improve fluidic flow detection such as optical, ultrasonic, and electrical sensing. When fluidic flow detection is based on the change of physical properties that are directly or indirectly related to electrical properties, the capacitively coupled contactless conductivity detection (C^4D) sensor structure [5-7] first proposed by A.J. Zemann, et al. (1998) [8]; J.A.F. da Silva, C.L. do Lago (1998) [9] is among the most prevalent methods. This method employs a conductivity detection technique in which a two-electrode configuration is utilized. These electrodes constitute a sensing capacitor including one electrode that acts as an exciting electrode in which the electrical signal is applied, and the other electrode function as a pick-up electrode where the electrical signal is sensed. Thus, any change in the electrical properties of the fluidic flow in the sensing area results in a change of the pick-up signal. This detection method has potential in many areas and has been employed in several detection and measurement applications [10-14]. However, stray capacitances can be generated by various sources, such as background noise, which can significantly influence the output sensitivity of the C^4D structure and thus impede the ability to detect objects or particles on the microscale.

Inductor-capacitor (LC) passive wireless sensing is based on the principle of resonance frequency shift detection. This is a high sensitivity technique that has been applied in several applications such as speed, position, and pressure detection [15, 16]. A potential technique to overcome the limits and difficulties of the conventional C^4D structure is its integration with LC sensing, resulting in a passive capacitively coupled contactless conductivity detection (PC^4D) sensor [17]. In this study, the C^4D structure, which acts as the sensing component, was connected to a PCB planar helical inductor to constitute a detection path whose resonant frequency is utilized for fluidic flow detection. LC sensors require no direct power connection to electrodes, thus minimizing any inadvertent change in electrical and chemical properties of the measured fluidic flow. The C^4D structure, as well as the planar inductors, were successfully fabricated using PCB technology. The fabricated PCB-based PC^4D structure was experimentally examined and the performance of the proposed method was evaluated by detecting the conductivity of the fluid and the presence of foreign objects in the fluidic flow.

2. Working principle and design

Figure 1A shows the design of the proposed PCB-based PC^4D sensor for fluidic flow detection. The proposed structure comprises two through-hole electrodes enclosing the conduit or the insulating pipe that contains the fluidic flow to be measured. The two electrodes create a sensing capacitor with the materials inside the channel wall acting as the dielectric material (Fig. 1B). An equivalent electrical circuit of the C^4D structure is shown in Fig. 1C. The resistance of the fluid inside the channel is R_S. The

*Corresponding author: Email: locdq@hus.edu.vn

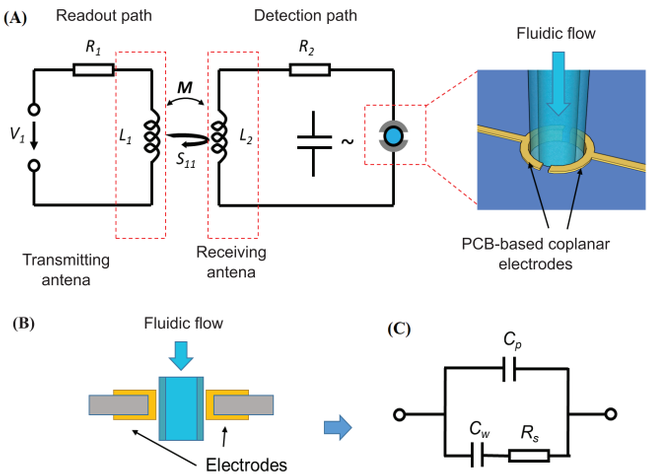

Fig. 1. Design of the proposed PCB-based PC⁴D sensor (A), a cross-section of a C⁴D structure (B), and the simplified equivalent circuit of the C⁴D structure (C).

wall capacitance is C_w. The configuration of the two electrodes also creates a stray capacitance C_p. Therefore, the impedance of the C⁴D cell, Z, can be determined by Q.L. Do, et al. (2019) [17]:

$$Z = \frac{R_S C_w^2 \omega^2 - j\left[\omega\left(C_w + C_p\right) + R_S^2 C_w^2 C_p \omega^3\right]}{\left(R_S C_p C_w w^2\right)^2 + \left[\omega\left(C_w + C_p\right)\right]^2} \quad (1)$$

where R_S is the solution resistance; $\omega=2\pi f$, f is the measurement frequency; j is the imaginary unit. As can be seen from the above equation, the imaginary part of the impedance is a function of ω, C_w, C_p, and R_s. The wall capacitance C_w depends on the dielectric layer's thickness and permittivity and the electrode's size. Thus, any change in the permittivity of the fluid material inside the conduit would give rise to a change in impedance of the sensing capacitor formed by the two electrodes.

As discussed above, two electrodes in the C⁴D structure constitute a capacitor with the dielectric material being the fluid flow. The sensing capacitor is connected to an inductor L_2, forming an LC resonator. The resonant frequency f_{res} of the detection path and quality factor Q can be expressed as Q.L. Do, et al. (2019) [17]:

$$f_{res} = \frac{1}{2\pi\sqrt{L_2 C}} \quad (2)$$

$$Q = \frac{1}{R_2} \times \sqrt{\frac{L_2}{C}} \quad (3)$$

where C is the capacitance of the sensing component in the detection path. The presence of an object or a change in the conductivity of the fluid gives rise to a change in the capacitance of the sensing capacitor. This in turn leads to a change in the resonant frequency of the LC resonator. The detection path is then wirelessly connected to the network analyser via a pair of antennae to detect such a change. The primary inductor L_1 works as the transmitting antenna. This antenna functions as the energy transmitting terminal by sending signals to the receiving antenna, which is the receiving inductor L_2 at the detection path with the C⁴D structure. The electrical signals from the network analyser are reflected through the pair of transmitting and receiving inductors. R_1 and R_2 are the parasitic resistances of the inductors. The input impedance Z_i of the network analyser is the combination of the reader path impedance Z_R and the detection path impedance Z_d, which is given by Q.L. Do, et al. (2019) [17]:

$$Z_i = Z_R + Z_d = R_1 + j\omega L_1 + \frac{(\omega M)^2}{R_2 + j\omega L_2 - j\left(\frac{1}{\omega C}\right)} \quad (4)$$

where ω is the angular frequency; R_1 and L_1 are the resistance and inductance of the readout coil, respectively; M is the mutual inductance between the transmitting antenna and the receiving antenna. The mutual inductance M of the coil is given by Q.A. Huang, et al. (2016) [18]:

$$M = k\sqrt{L_1 L_2} \quad (5)$$

where k is the geometry-dependent coupling coefficient with a value that varies between 0 (no coupling) and ±1 (maximum coupling).

As can be seen from Eq. 4, with the values of the primary and secondary inductors (L_1 and L_2) and the mutual inductance M between two coils considered constant during the measurement, the input impedance to the network analyser Z_i depends on the capacitance of the C⁴D sensor as well as the operating frequency. The input impedance of the detection path will experience changes corresponding to a change of the fluidic flow. This results in a change of the input reflection coefficient S_{11}, i.e., the ratio of reflected and incident power. As the excitation frequency corresponds to the resonant frequency of the LC detection path, the reflection coefficient S_{11} hits a low. Therefore, the change in the resonant frequency of the LC circuit can be detected by analysing the reflection coefficient S_{11}.

3. Measurement setup

Figure 2A shows the experimental measurement setup. A network analyser (E5061A, ENA Agilent) was used as a vector network analyser to detect the resonant frequency of the LC wireless passive sensor by analysing the reflection coefficient S_{11}. At the resonant frequency of the detection path, the parameter S_{11} reaches a minimum value. The fluidic channel was a silicon tube. A syringe micropump (AS ONE - CT10) was used to inject the solution into the fluidic channel. In addition, several experiments were conducted to determine the resonance frequency change while air bubbles move through the detection zone. The Y-channel configuration was employed in conjunction with two syringes. One syringe contained a sodium chloride (NaCl) solution, while the other was filled with air. As the micropump was activated, liquid droplets and air bubbles were generated inside the main channel. By altering the liquid and air phase flow rate, liquid droplets and air bubbles of different sizes can be achieved.

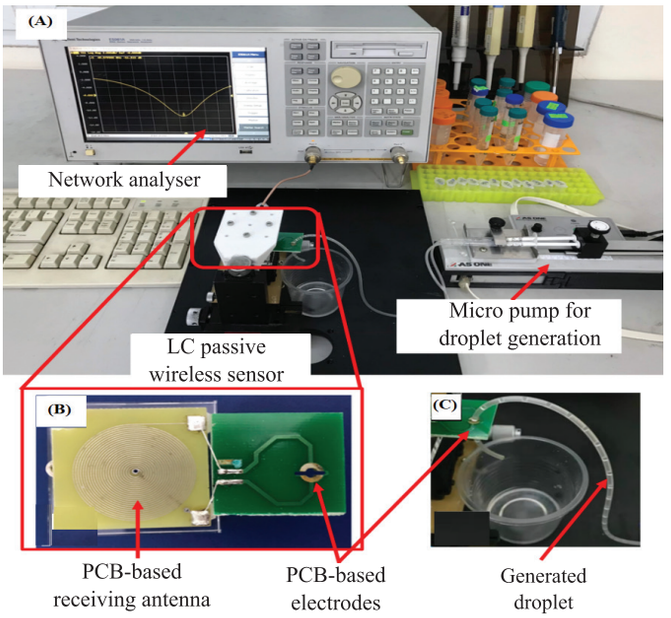

Fig. 2. Measurement setup (A), the fabricated detection path including the receiving antenna and the PCB-based electrodes of the C⁴D structure (B), and the experimental generated droplets (C).

Both the electrodes of the C⁴D structure as well as the primary and secondary inductors were fabricated by the (PCB) technique. Fig. 2B shows the design of the transmitting and receiving antennae as well as the design of the two electrodes that constitute the sensing component of the C⁴D structure. The electrodes of the C⁴D structure were designed as through-hole semicircles facing each other. Each electrode has an inner radius of 1.15 mm and an outer radius of 2.5 mm. The two electrodes are separated by a cavity where the fluidic channel is placed for measurements, as shown in Fig. 2C. Similar to the capacitance sensing electrodes, the receiving antenna was designed as helical coplanar inductors on a PCB board. The inductor at the detection path has a radius of 12.3 mm, which is composed of 23 turns, as shown in Fig. 2B. Meanwhile, the transmitting antenna has a dimension of 20x20 mm with a width of 1 mm. Two inductors are placed in air and separated by a fixed distance of 8.0 mm.

4. Results and discussion

4.1. Fluidic flow conductivity detection

NaCl solutions with concentrations ranging from 10 mM to 1 M were utilized to examine the ability to detect changes in the conductivity of the fluid flow. The network analyser detects the resonant frequency of the detection path by parametrically sweeping the stimulating frequencies. The reflection coefficient S_{11} corresponding to the sweeping frequency of the excitation signals was acquired. At the resonant frequencies, the reflection coefficient S_{11} experiences a minimum. Fig. 3A shows the relationship between the reflection coefficient S_{11} and the stimulating frequency with several values of the NaCl concentration solution. In the experiments with each concentration, the acquired values of resonant frequency at which S_{11} was a minimum were extracted. The experimental results show that when the concentration of the NaCl solution filling the fluidic channel increases from 10 mM to 1 M, the resonant frequency of the proposed sensor decreases from 49.32 to 49.12 MHz, respectively. At the same time, the value of the reflection coefficient S_{11} changes from -10.04 to -11.01 dB. Therefore, it can be concluded that the change in the measured solution not only caused a shift in the resonant frequency but also the value of the reflection coefficient S_{11}. Fig. 4 also demonstrates that the resonant frequency varies with the concentration of the solution. On a logarithmic scale of NaCl concentration, the dependence of the resonant frequency on the NaCl concentration is considered roughly linear with a decreasing rate of approximately 0.098 MHz/decade. Therefore, it is possible to utilize the proposed LC wireless passive sensor to detect the

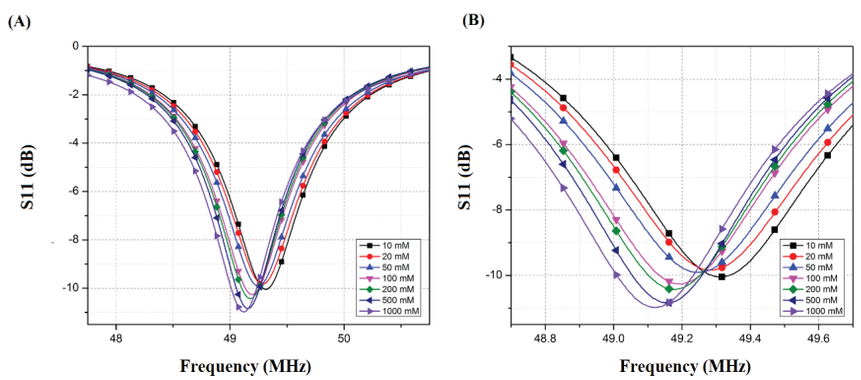

Fig. 3. Dependence of the reflection coefficient S_{11} on the NaCl concentration ranging from 10 mM to 1 M over frequencies ranging from 48 to 50.5 MHz (A) and over the frequency range from 48.8 to 49.8 MHz (B).

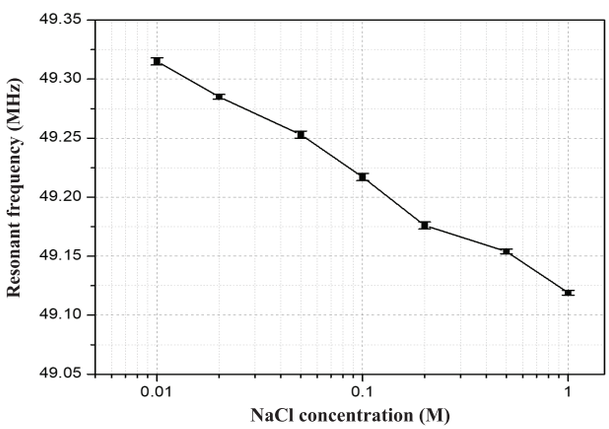

Fig. 4. The dependence of the resonant frequency on the concentration of NaCl solution.

electrical properties of the solution by measuring the resonant frequencies of the detection path.

4.2. Detection of liquid drops and air bubbles passing through the sensor

An air bubble generation structure utilizing a Y-junction configuration was conducted to investigate the ability to detect the appearance of foreign objects in the fluidic flow. Two syringes with a volume of 1 ml were employed to generate the same flow rate for the two phases. The syringe micropump speed was set at 6 mm/min. With such configurations, the length of the droplets and air bubbles generated in the main channel were equal. The resonance frequency of the detection path was monitored and tracked while air bubbles and droplets moved along the main fluidic channel through the detection zone.

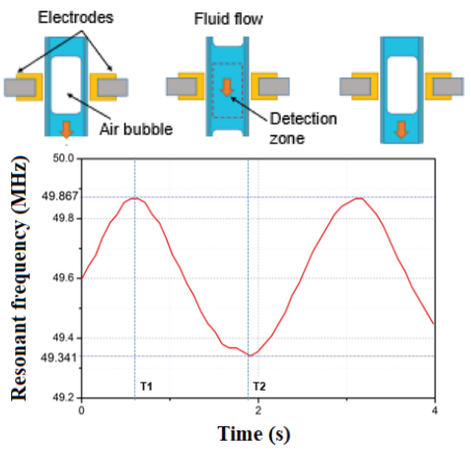

Fig. 5. Resonant frequency of the detection path as bubbles pass through the detection zone with the channel filled with 1 M NaCl.

The alternation of the resonant frequency according to the passage of air bubbles through the detection zone is shown in Fig. 5. The results show the resonant frequency's dependence on air bubble position inside the fluidic channel, which causes a change in the resonance frequency of the detection path circuit. When the droplets and air bubbles pass through the sensing region of the C^4D structure, the measured resonant frequency of the detection path changes. As the air bubbles travel through the detection region at T_1, the acquired resonant frequency increases. In contrast, the resonant frequency value drops at the appearance of liquid droplets passing the detection zone (T_2). Since the Y-junction droplet generation configuration generates air bubbles and liquid droplets consecutively, the acquired resonant frequency changed harmonically. These primary results demonstrate that the detection system can recognize the appearance of foreign objects or air bubbles. Compared to the C^4D technique proposed by X.Y. Tang, et al. (2020) [19], which used the C^4D technique with capacitive reactance elimination, the LC passive wireless detection method appears to be more precise. The observed data seems to be less influenced by background noise. In addition, this flow detection approach does not require a complex circuit for signal conditioning or a processing unit.

Object detection performance of the proposed system was experimentally studied. The sizes of droplets and air bubbles were altered by modifying the input flow rate into the Y junction. The length ratio (LR) of a generated droplet is defined as the ratio of the length of the liquid droplet over the length of an air bubble generated in the main fluidic channel:

$$LR = \frac{L_{liquid\ droplet}}{L_{air\ bubble}} \quad (6)$$

In this study, two syringes of different volumes, including 1 and 3 ml, were employed to produce a LR of approximately 1:5. Fig. 6 shows the variation of resonant frequency in the detection path when 1 M NaCl droplets and air bubbles passed through the sensor with LRs of 1:1 and 1:5. It can also be seen from the results that in the case of LR=1:5, the average value of resonant frequency was higher than that of LR=1:1. In the case of LR=1:5, the resonant frequencies varied from approximately 49.5 to 50.25 MHz. Meanwhile, the resonant frequencies changed in the range of 49.34 and 49.85 MHz in the case of LR=1:1. In addition, it can also be observed that the peak of the signals with LR=1:5 lasted longer than the minimum signal peaks at LR=1:1. This can be explained by the fact that the air bubbles were longer in the case of LR=1:5. Therefore, it took the air bubbles more time to pass through the detection zone, which resulted in the maximum peaks of the acquired signals lasting longer.

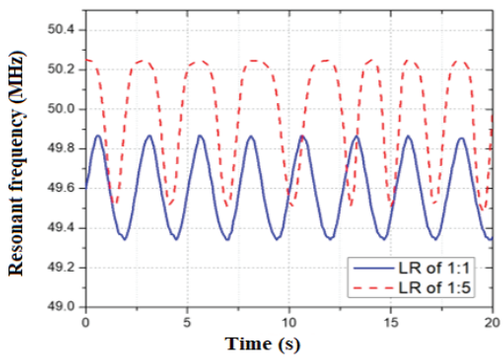

Fig. 6. The acquired resonant frequency of the system with 1 M NaCl droplet-air bubble experiments with LRs of 1:1 and 1:5.

With each LR value, the influence of solution concentration was studied. Specifically, five concentrations of the NaCl solution, including 0.01, 0.05, 0.1, 0.5, and 1 M, were investigated. The resonant frequencies reached a minimum when the NaCl droplets passed through the sensor. This passage corresponds to the minimum peaks of the acquired resonant frequency. Fig. 7A shows the dependence of the resonant frequency minima on the concentration of NaCl solution with LRs of 1:1 and 1:5, respectively.

In the case of LR=1:1, the passage of 0.01 M NaCl droplets resulted in a resonant frequency of 49.419 MHz. As the NaCl droplet concentration increased, the minimum peak values also decreased on a logarithmic scale with a rate of 0.041 MHz/decade. The minimum was approximately 49.338 MHz with the passage of

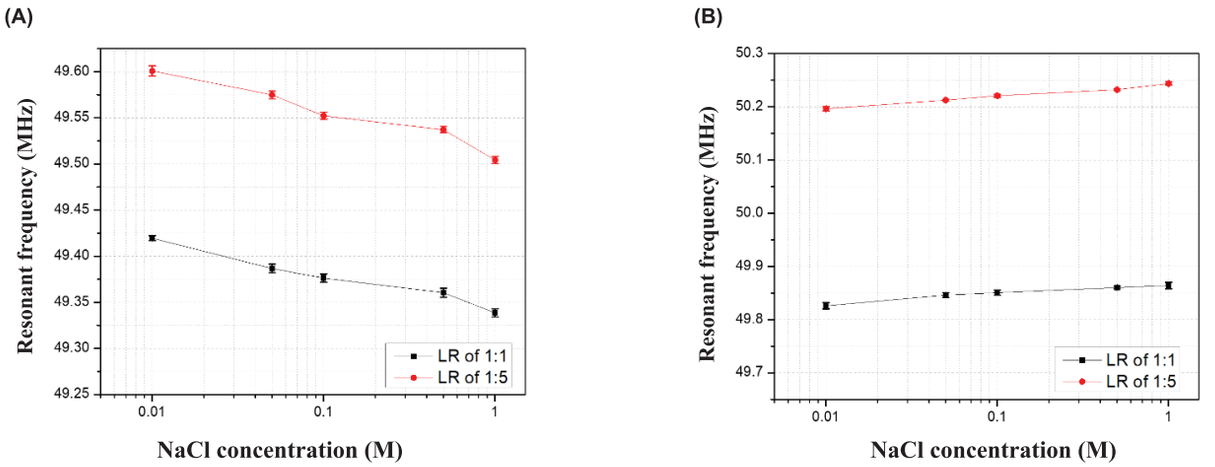

Fig. 7. Dependence of minimum (A) and maximum (B) peaks on the concentration of NaCl with the LR of 1:1 and 1:5.

1 M NaCl droplets. Similarly, the passage of 0.1 M NaCl droplets with LR=1:5 resulted in a minimum peak of 49.504 MHz, while the 1 M NaCl droplets resulted in a resonant frequency of 49.5043 MHz with the declining rate being 0.048 MHz/decade. In contrast, when the concentration of NaCl increased, the resonant frequency maxima corresponding to the passage of air bubbles through the detection zone increased as well, as shown in Fig. 7B. The maximum peak value for LR=1:1 was 49.8259 MHz with 0.01 M NaCl droplets. As the NaCl concentration grew to 1 M, the resonant frequency increased to 49.864 MHz with a rate of 0.0192 MHz/decade. Meanwhile, the maximum resonant frequency also increased with the NaCl concentration, but at a higher rate of 0.0237 MHz/decade in the case of LR=1:5. It can be seen from both Fig. 7A and Fig. 7B that the increase of resonant frequency with molar concentration is less significant when measuring maximum peaks. This is because peak maxima represent the appearance of air bubbles, as illustrated in Fig. 5, thus, if the air bubble already occupies a large area of the detection region, the concentration of NaCl does not have much influence.

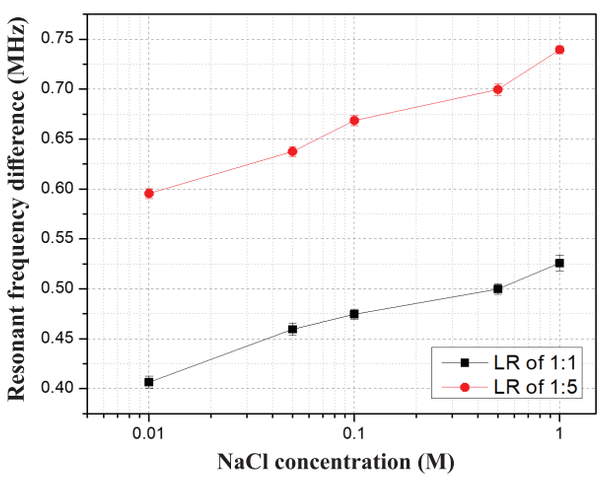

Fig. 8. Difference between maximum and minimum peaks of the resonant frequencies according to the passage of NaCl droplets at different LRs.

Figure 8 shows the difference between maximum and minimum peaks (Δ_{fres}) of the resonant frequencies according to the passage of NaCl droplets at different LRs. As can be seen from the graph, the differences, given by Δ_{fres}, for LR=1:1 and 1:5 seem to be quite clear. The frequency gap between the signal of LR=1:1 and LR=1:5 is approximately 0.18 MHz. As the NaCl concentration increased, Δ_{fres} also increased in both cases. At the same time, the frequency gap broadened but not significantly. It can be implied that Δ_{fres} certainly indicates the ratio between the length of droplets and air bubbles as well as the conductivity of the droplets. Although the proposed system is currently limited in characterizing different substances in the fluidic flow, the difference in Δ_{fres} in these experiments has demonstrated that implementation of the resonant frequency of the proposed sensing structure comprising the C^{4}D structure coupled with a coplanar inductor can detect not only the conductivity of the solution but also the size and electrical conductivity of the particles or objects inside the fluidic channel.

5. Conclusions

This paper proposed and developed a PCB-based PC^{4}D sensor for fluidic flow detection. The sensing structure integrates a C^{4}D structure with a coplanar inductor to form a detection path with its resonant frequencies varying with fluid flow. The obtained results show that the conductivity of the fluidic flow can be determined by measuring the resonant frequency of the detection path utilizing the reflection coefficient S_{11}. The resonant frequency experiences a linear increase according to the increase in the electrical conductivity of the fluidic flow. Experiments were also carried out to investigate droplet-air bubble detection. The frequency gap between the case of LR=1:1 and LR=1:5 was approximately 0.18 MHz. The experimental results indicated that by using the proposed method, the size and electrical conductivity of the particles or objects inside the fluidic flow could be estimated. The results show this scheme has great potential for use in various applications in biomedical and chemical fields but especially in biomedical applications.

CRediT author statement

Nhu Cuong Nguyen: Simulation Implementation, Writing the manuscript; Bao Anh Hoang: Experiment implementation; Trung Kien Do: Data analysis, Data presentation; Thanh Tung Bui: Supporting data analysis, Literature review; Duc Trinh Chu: Review manuscript and Supervise the project; Quang Loc Do: Supervise and Editing.

ACKNOWLEDGEMENTS

This research is funded by Vietnam National Foundation for Science and Technology Development (NAFOSTED) under grant number 103.99-2020.40.

COMPETING INTERESTS

The authors declare that there is no conflict of interest regarding the publication of this article.

REFERENCES

[1] A.L. Campana, S.L. Florez, M.J. Noguera, et al. (2019), "Enzyme-based electrochemical biosensors for microfluidic platforms to detect pharmaceutical residues in wastewater", *Biosensors*, **9(1)**, DOI: 10.3390/BIOS9010041.

[2] S. Motomizu (2012), "Computer-controlled fluid-flow chemical analysis (CC-FCA) and its application to environmental analytical chemistry", *Pure and Applied Chemistry*, **84(10)**, pp.1999-2013, DOI: 10.1351/PAC-CON-12-02-09.

[3] D. Janasek, J. Franzke, A. Manz (2006), "Scaling and the design of miniaturized chemical-analysis systems", *Nature*, **442(7101)**, pp.374-380, DOI: 10.1038/nature05059.

[4] P. Sengupta, K. Khanra, A.R. Chowdhury, et al. (2019), "Lab-on-a-chip sensing devices for biomedical applications", *Bioelectronics and Medical Devices: From Materials to Devices - Fabrication, Applications and Reliability*, pp.47-95, DOI: 10.1016/B978-0-08-102420-1.00004-2.

[5] W.K.T. Coltro, R.S. Lima, T.P. Segato, et al. (2012), "Capacitively coupled contactless conductivity detection on microfluidic systems - Ten years of development", *Analytical Methods*, **4(1)**, pp.25-33, DOI: 10.1039/C1AY05364G.

[6] P. Kuban, P.C. Hauser (2011), "Capacitively coupled contactless conductivity detection for microseparation techniques - recent developments", *Electrophoresis*, **32(1)**, pp.30-42, DOI: 10.1002/ELPS.201000354.

[7] P. Kuban, P.C. Hauser (2008), "A review of the recent achievements in capacitively coupled contactless conductivity detection", *Analytica Chimica Acta.*, **607(1)**, pp.15-29, DOI: 10.1016/j.aca.2007.11.045.

[8] A.J. Zemann, E. Schnell, D. Volgger, G.K. Bonn (1998), "Contactless conductivity detection for capillary electrophoresis", *Anal. Chem.*, **70(3)**, pp.563-567, DOI: 10.1021/ac9707592.

[9] J.A.F. da Silva, C.L. do Lago (1998), "An oscillometric detector for capillary electrophoresis", *Anal. Chem.*, **70(20)**, pp.4339-4343, DOI: 10.1021/ac980185g.

[10] T.V. Quoc, H.N. Dac, T.P. Quoc, et al. (2015), "A printed circuit board capacitive sensor for air bubble inside fluidic flow detection", *Microsystem Technologies*, **21(4)**, pp.911-918, DOI: 10.1007/s00542-014-2141-8.

[11] H.N. Dac, H.T.T. Thuy, T.V. Quoc, et al. (2020), "Study on design optimization of a symmetry two-axis tilt angle capacitive sensor", *IETE J. Res.*, **69(1)**, pp.264-271, DOI: 10.1080/03772063.2020.1816224.

[12] A.A. Elbashir, H.Y. Aboul-Enein (2010), "Applications of capillary electrophoresis with capacitively coupled contactless conductivity detection (CE-C4D) in pharmaceutical and biological analysis", *Biomedical Chromatography*, **24(10)**, pp.1038-1044, DOI: 10.1002/bmc.1417.

[13] K.A. Mahabadi, I. Rodriguez, C.Y. Lim, et al. (2010), "Capacitively coupled contactless conductivity detection with dual top - bottom cell configuration for microchip electrophoresis", *Electrophoresis*, **31(6)**, pp.1063-1070, DOI: 10.1002/elps.200900578.

[14] J.P. Hutchinson, C. Johns, M.C. Breadmore, et al. (2008), "Identification of inorganic ions in post-blast explosive residues using portable CE instrumentation and capacitively coupled contactless conductivity detection", *Electrophoresis*, **29(22)**, pp.4593-4602, DOI: 10.1021/ac2020195.

[15] H. Wen, C. Chen, S. Li, et al. (2021), "Array integration and far-field detection of biocompatible wireless LC pressure sensors", *Small Methods*, **5(3)**, DOI: 10.1002/SMTD.202001055.

[16] C.S. Lee, C.Y. Wu, Y.L. Kuo (2017), "Wearable bracelet belt resonators for noncontact wrist location and pulse detection", *IEEE Transactions on Microwave Theory and Techniques*, **65(11)**, pp.4475-4482, DOI: 10.1109/TMTT.2017.2684118.

[17] Q.L. Do, T.T. Bui, B.A. Hoang, et al. (2019), "Development of a passive capacitively coupled contactless conductivity detection (PC4D) sensor system for fluidic channel analysis toward point-of-care applications", *IEEE Sensors Journal*, **19(15)**, pp.6371-6380, DOI: 10.1109/JSEN.2019.2908179.

[18] Q.A. Huang, L. Dong, L.F. Wang (2016), "LC passive wireless sensors toward a wireless sensing platform: Status, prospects, and challenges", *Journal of Microelectromechanical Systems*, **25(5)**, pp.822-841, DOI: 10.1109/JMEMS.2016.2602298.

[19] X.Y. Tang, J. Huang, H. Ji, et al. (2020), "New method for bubble/slug velocity measurement in small channels", *Review of Scientific Instruments*, **91(5)**, DOI: 10.1063/1.5134548.